EXPERIMENTAL ANALYSIS TO IDENTIFY THE DEFORMATION MECHANISMS DURING SINTERING OF COLD COMPACTED POLYTETRAFLUOROETHYLENE (PTFE) POWDERS

Rodrigo B. Canto, Nicolas Schmitt, Jonas Carvalho, René R. Billardon

EXPERIMENTAL ANALYSIS TO IDENTIFY THE DEFORMATION MECHANISMS DURING SINTERING OF COLD COMPACTED POLYTETRAFLUOROETHYLENE (PTFE) POWDERS

R. B. Canto[1,2,*], N. Schmitt[1,3], J. Carvalho[2], R. Billardon[1]

[1]LMT-Cachan (ENS de Cachan/CNRS (UMR 8535)/UPMC (Univ. Paris 6))
61, avenue du Président Wilson F-94235 Cachan, France
Nicolas.Schmitt@lmt.ens-cachan.fr; Rene.Billardon@lmt.ens-cachan.fr
[2]Escola de Engenharia de São Carlos (EESC-USP)
Av. Trabalhador São Carlense, 400 - São Carlos-SP, Brasil
canto@sc.usp.br*; prjonas@sc.usp.br
[3]Université Paris 12 Val de Marne (PRES Paris-Est)
Place du 8 Mai 1945, F-93203 Saint-Denis, France

Abstract – Thermal dilatometry analyses were performed on specimens made of pure or filled PTFE powders. The specimens were obtained by isostatic pressing or by uniaxial compaction up to different values of the residual void ratio. The large deformations that were recorded during different heating-cooling treatments strongly depend on the mode and level of compaction, as well as on the presence or the absence of fillers. Besides, these deformations are strongly anisotropic when the specimens are obtained by uniaxial compaction. It has been shown that this macroscopic deformation observed during sintering results from the combination of different mechanisms, viz. thermal expansion, recovery, void closure, crystalline to amorphous phase change and vice versa, that were identified by varying the heat treatments.

Keywords: dilatometry, strain mechanisms, void closure, recovery, crystallisation, compaction.

1 Introduction

Since high molecular weight polymers such as poly(tetrafluoroethylene) (PTFE) are not melt-processible because of their very high melt viscosities, parts made of these materials are frequently manufactured by room-temperature powder compaction followed by a heat treatment [1] commonly referred to as “sintering” [2]. It can be noticed that powder processing may help and limit the number of machining operations that are necessary to obtain the accurate dimensions of the final product. Moreover, the physical and mechanical properties of the finished PTFE parts are strongly dependent on various parameters of the manufacturing process [3].

During compaction, the material – i.e. a compound of lamellar crystalline grains, amorphous phase and, in some cases, different types of fillers – undergoes very large plastic strains that may induce a local 'texture' of the material, viz. an orientation of the molecular chains, crystalline grains and fillers. Sintering process corresponds to heating up above the melting temperature, holding on and cooling down to room temperature the so-called green material – i.e. the compacted powder with a certain degree of remaining porosity. During the sintering process, the green material undergoes large deformations that are generally anisotropic.

The macroscopic sintering deformation is the result of different mechanisms which may depend on the texture of the green material and hence, on the mechanical load applied during the compaction process. The objective of the work presented herein is to identify these different mechanisms. This work is part of a study the ultimate aim of which is to build a predictive model of

* corresponding author, now at DEMa/UFSCar (Universidade Federal de São Carlos, SP, Brasil)

the deformations of PTFE parts during their manufacturing process in order to better control this compaction and sintering process. Some works have dealt with the compaction of polymer powders [4-8] and other works with the sintering of polymers [2-3, 9-14], in particular PTFE [1, 7, 15-16]. However, to the authors' knowledge, no published paper describes in details the strain mechanisms developed during the sintering of a PTFE compacted powder.

2 Experiments

2.1 Materials

This study is mainly dedicated to a pure PTFE powder, supplied as Teflon® PTFE 6407. A few tests have also been performed on a filled PTFE powder with carbon fibers and ekonol®. The size of the pellets varies between 400 and 1000 μm for the pure material and between 300 and 1000 μm for the filled material.

A ThermoGravimetric Analysis (TGA) of both materials was made at 10 °C/min heating rate with a DSC Q1000 *TA Instruments*™ apparatus. In N_2 inert atmosphere, the analyses reveal that there is no significant mass loss in the pure material below 400°C. This result is in agreement with the results given in ref. [17] where a small mass loss rate of about 3.10^{-5} %/min was reported at 390 °C. The mass loss rate reaches 0.01 %/min at 425 °C and a maximum value of 20 %/min at 575 °C. In an oxidative atmosphere composed of 20 % of O_2 and 80 % of N_2, the temperature corresponding to the initiation of mass loss is not altered, and a maximum rate of 20 %/min occurs at a lower temperature, viz. 550 °C. In N_2 inert atmosphere, the mass loss of the filled material occurs with a rate of 0.01 %/min at 390 °C and with a maximum value of 22 %/min at 565 °C. These analyses demonstrate the importance of the maximum temperature that is recommended for the sintering process, viz. between 360 °C and 380 °C in order to avoid significant degradation of the material [18].

Differential Scanning Calorimetry (DSC) analyses of the pure PTFE powder were carried out on 5 mg of as-delivered pure PTFE powder with a DSC Q1000 *TA Instruments*™ apparatus. A typical DSC plot obtained on a specimen initially cooled to – 50 °C, heated up to 400 °C at 10 °C/min, maintained at this temperature for 5 min, and then cooled down at – 10 °C/min is given in Figure 1.

Different microstructural transformations are observed. The heat flow peaks around the room temperature correspond to allotropic transformations of PTFE crystals [19]. During heating, a crystallographic change from triclinic (phase II) to hexagonal (phase IV) occurs at 19 °C leading to a specific mass decrease of 1 % [18]. Another crystallographic change to pseudo-hexagonal (phase I) occurs at 30 °C. Considering that the deformations induced by these solid/solid tranfromations at atmospheric pressure are negligible when compared to macroscopic sintering deformations, they are ignored herein. It can be noticed that the orthorhombic configuration (phase III) occurs at pressures higher than about 500 MPa so that it is not usually encountered in conventional processing.

The endothermic peak observed at 344 °C during heating corresponds to the melting of the original crystalline phase. At this heating rate, melting starts at about 325 °C and is complete at about 355 °C. During this stage, the crystalline phase disappears progressively and the material becomes completely amorphous – with a very high viscosity reported between 10^{10} Pa.s [20] and

10^{11} Pa.s [21]. The peak observed during cooling at 316 °C corresponds to a partial crystallisation of the material the rate of which becomes negligible below 240 °C.

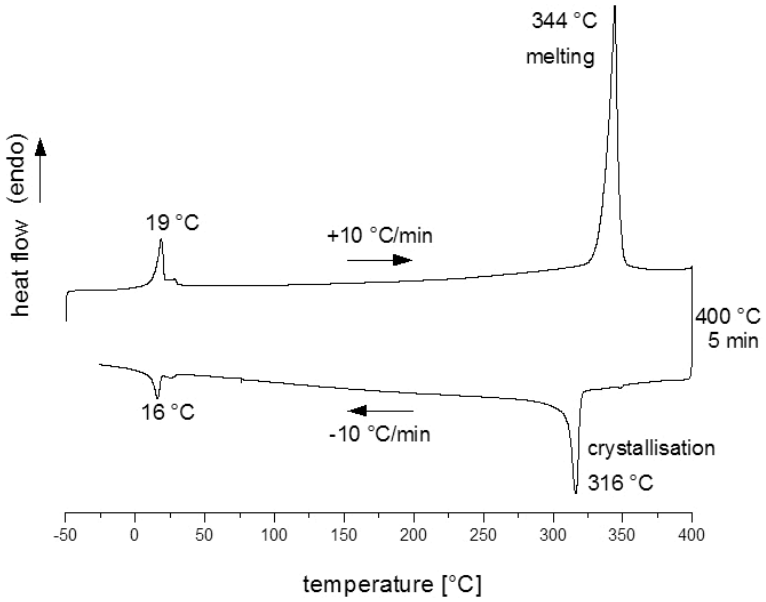

Figure 1 – DSC plot of pure PTFE

A complex DSC test with the cyclic thermal loading given in Figure 2 has been performed. This test allows the evaluation of the degree of crystallinity as a function of the cooling rate.

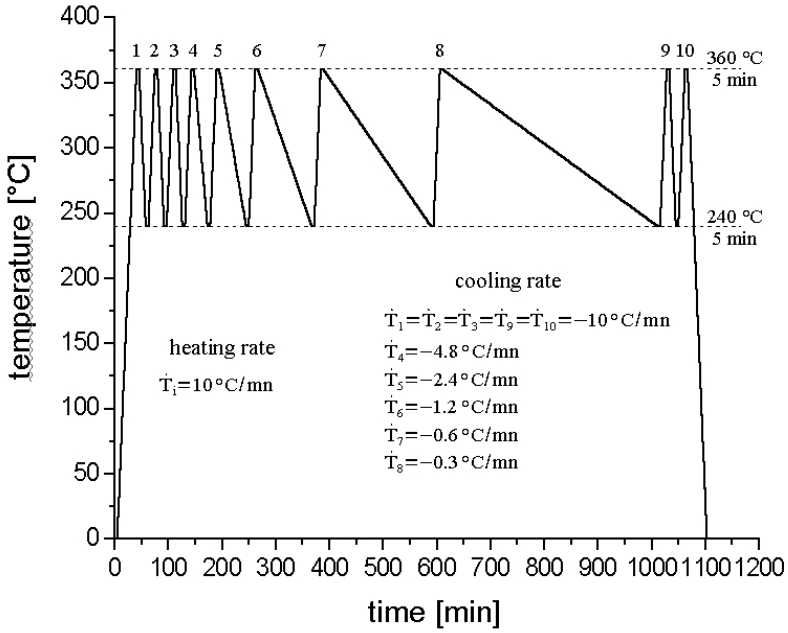

Figure 2 – Thermal loading applied during a cyclic DSC test

Plots of the melting peaks for cycles 1, 2, 3, 4 and 10 performed at the same heating rate, viz. 10 °C/min, but at different cooling rates, are shown in Figure 3. As reported by many authors [17, 22-23], the melting associated with the crystalline phase formed after the first melting – i.e. when heating sintered material – differs from the melting of the original crystalline phase and appears at a lower temperature (about 327 °C). Besides, the area under the different DSC peaks

proves that the crystalline weight fraction of the as-delivered material is much higher than the crystalline weight fraction of the sintered material. The plots related to cycles 2, 3 and 4 show that, after the first melting, the microstructural changes can be considered as approximately reversible. The plot related to cycle 10 presents a 9 % larger area than those obtained for cycle 4. Considering an uncertainty of about ± 3% related to the choice of a baseline, this result could be associated to a small degradation of the material due to its long exposure to high temperatures during cycles 5 to 9. Indeed, according to ref. [24], above 360 °C, degradation of PTFE leads to a lower molecular weight and hence, to higher values of the degree of crystallinity. However, cyclic tests were used herein in order to avoid uncertainties associated to measurements made on different samples.

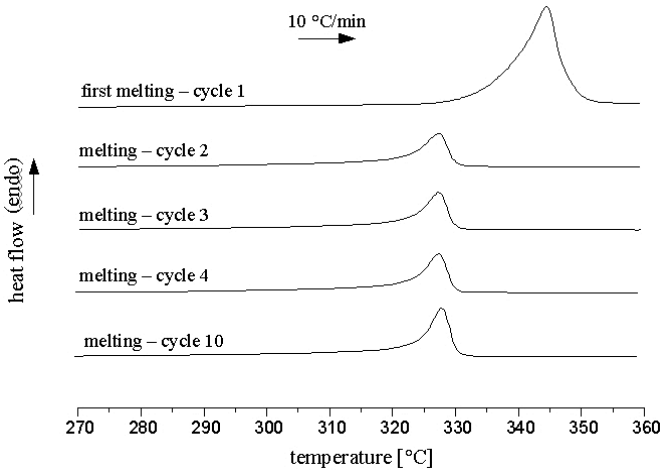

Figure 3 – Melting peaks during a cyclic DSC test on pure PTFE.

2.2 Methodology to compact samples and to perform dilatometry tests

Different green samples of pure or filled PTFE were manufactured by isostatic pressing or confined uniaxial (or oedometric) compaction. After several days of natural creep at room temperature, these samples were subjected to different heat treatments in a SETSYS *SETARAM*™ dilatometer while measuring their deformation – the load applied on the probe being controlled as $2\ 10^{-4}$ N. The cylindrical specimens that were obtained by isostatic pressing (see Figure 4) are referred to as isotropic specimens so that their deformation is measured in only one direction. The parallelepiped shaped specimens that were obtained by uniaxial compaction (see Figure 5) are referred to as anisotropic specimens so that for each set of compaction parameters and subsequent heat treatment the deformation of two different specimens was measured in the compaction direction or in the perpendicular direction.

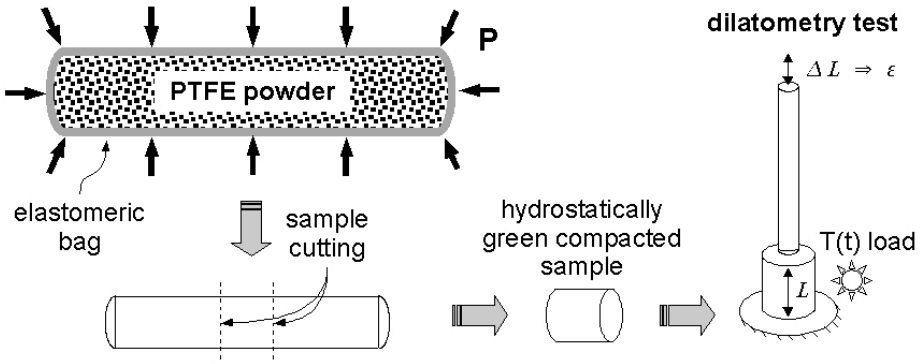

Figure 4 – Manufacturing process of isotropic samples by isostatic pressing.

Dimensions of the dilatometry specimens: diameter ~ 6 mm and height L_{oi} ~ 6 mm.

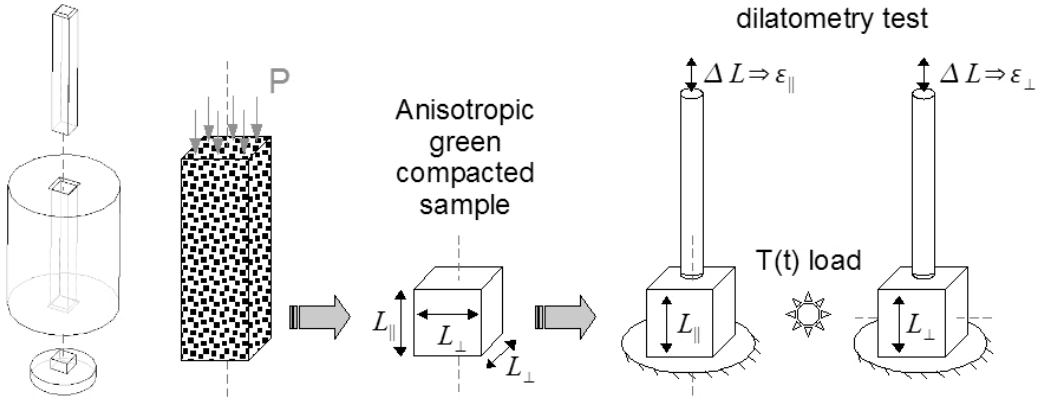

Figure 5 – Manufacturing process of anisotropic samples by confined uniaxial compaction. Dimensions of the dilatometry specimens: $L_{\perp i}$ = 8 mm, $L_{\parallel i}$ = 7.6 ~ 9 mm.

During the dilatometry tests, the measured strains are defined as

$$\varepsilon = ln\frac{L}{L_{oi}}, \quad \varepsilon_{\perp} = ln\frac{L_{\perp}}{L_{\perp i}} \quad \text{and} \quad \varepsilon_{\parallel} = ln\frac{L_{\parallel}}{L_{\parallel i}} \tag{1}$$

where L_{oi} and L_i respectively denote the current and the initial length of the specimen. Additionally, ε denotes the uniaxial strain of the isotropic samples, whereas $\varepsilon_{\perp}$ and $\varepsilon_{\parallel}$ respectively denote the uniaxial strain in the compaction direction and in the perpendicular direction of the anisotropic samples.

The volumetric strain of isotropic samples is computed as

$$\varepsilon_{vol} = 3\,\varepsilon \tag{2}$$

whereas the volumetric strain of anisotropic samples is computed as

$$\varepsilon_{vol} = \varepsilon_{\parallel} + 2\,\varepsilon_{\perp} \tag{3}$$

3 Results obtained on isotropic specimens

3.1 Evolution of the void ratio during compaction

Assuming that the pure material powder is made of three phases, viz. voids and amorphous or crystalline polymer material, the specific volume, v, and the specific mass, ρ, of any green material are defined by the following relationships

$$v = \frac{V_v + V_c + V_a}{m_c + m_a} \quad \text{and} \quad \rho = \frac{1}{v} \tag{4}$$

whereas the specific volume and specific mass of fully dense green material are defined by

$$v_S = \frac{V_C + V_a}{m_C + m_a} = \frac{V_S}{m_S} \quad \text{and} \quad \rho_S = \frac{1}{v_S} \tag{5}$$

where m_i and V_i respectively denote the mass and the volume of the voids ($i = v$), the solid ($i = s$) and of the amorphous ($i = a$) or crystalline ($i = c$) phases.

Consequently, the void ratio, e, of any green material can be derived from the measurement of its specific mass, ρ, which is defined as

$$e = \frac{V_V}{V_S} = \frac{V_V}{V_C + V_a} = \frac{\rho_S}{\rho} - 1 \tag{6}$$

Spherical isotropic green samples, about 35 mm in diameter, have been manufactured by isostatic pressing up to different values of the pressure. The specific mass of these isotropic green samples was obtained by direct measurements of their mass and volume. The variations of the final void ratio and specific mass with the maximum pressure applied when manufacturing these green isotropic specimens are plotted in Figure 6. From this result, it can be assumed that, for both pure and filled materials, the void ratio is approximately nil after a compaction up to about 140 MPa. This assumption is in good agreement with the literature [18, 25] and allows to measure the specific mass, ρ_S, of fully dense (or solid) material, as defined by Eq. (5).

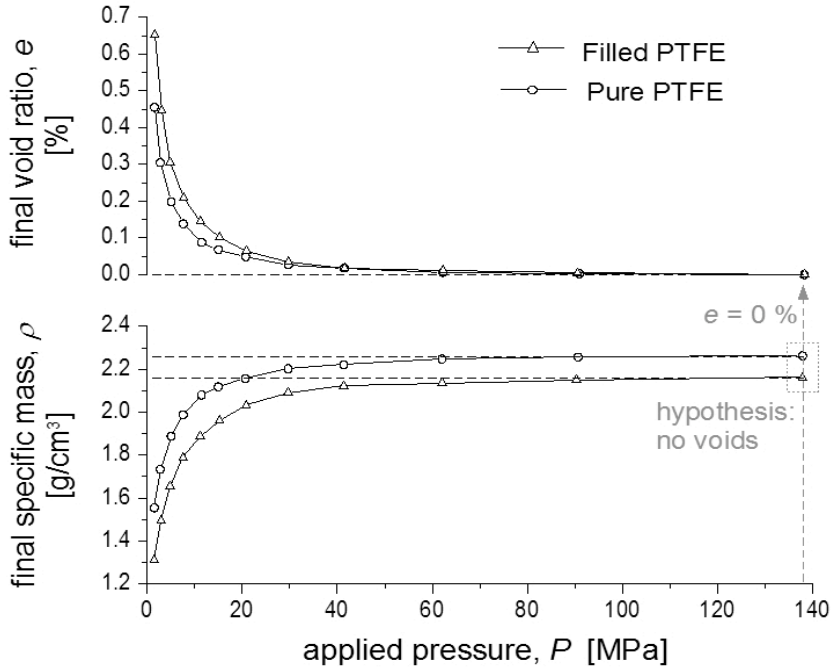

Figure 6 – Final void ratio and specific mass of green spherical samples made of pure PTFE obtained by isostatic pressing vs. maximum applied pressure during the manufacturing process.

3.2 Evolution of the crystalline weight fraction during sintering of pure PTFE

Assuming that the powder of pure material is made of three phases, viz. voids and amorphous or crystalline polymer material, the crystalline weight fraction defined as

$$\chi = \frac{m_C}{m_S} = \frac{m_C}{m_C + m_a} \tag{7}$$

can be derived from the following equation

$$v = (\chi\, v_c + (1 - \chi)\, v_a)\,(e + 1) \tag{8}$$

with the following values of the specific volume for the amorphous and crystalline phases [18]

$$v_a = 0.500 \text{ cm}^3/g \quad \text{and} \quad v_c = 0.435 \text{ cm}^3/g \tag{9}$$

Equations (8-9) allow to derive the value of the crystalline weight fraction of the green material from direct measurements of the specific volume of fully dense green samples. The value obtained for the pure PTFE studied herein is 89 wt%.

The crystalline weight fraction of the sintered material was derived from the results of the DSC cyclic test corresponding to Figure 2 by applying the following procedure:

i) the area under the melting peak subsequent to cooling at a given cooling rate was calculated with a linear baseline between 270 and 345 °C;

ii) the value of this area was divided by the value of the area of the melting peak of the virgin material (cycle 1), which was calculated with a linear baseline between 270 and 360 °C;

iii) the crystalline weight fraction was then obtained considering that the virgin material is 89 wt% in crystallinity – according to the specific mass measurements.

The influence of the cooling rate – after complete melting – on the value of the crystalline weight fraction derived from DSC tests following the above-described procedure is illustrated by Figure 7. On the same figure, these results are compared to the values that were derived from equations (8-9) applied to nil void ratio sintered samples (with a mass of about 0.4 g) the specific mass of which was measured by using Archimedes's principle.

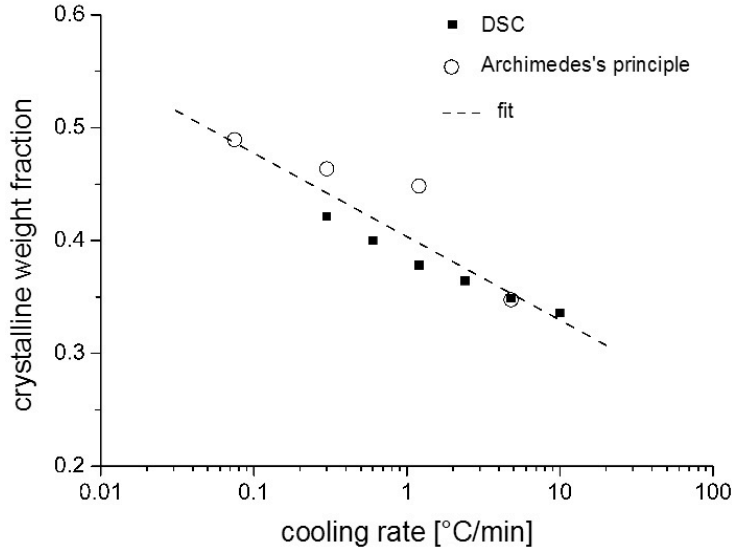

Figure 7 – Crystalline weight fraction vs. cooling rate for pure PTFE

The results given in Figure 7 can be fitted with the following equation

$$\chi = 0.27 - 0.074\, log_{10}\, \dot{T} \tag{10}$$

where $\dot{T}$ is given in K/s.

3.3 Identification of deformation mechanisms during sintering of pure PTFE

The results given in Figure 8 correspond to dilatometry tests which were performed while applying a typical sintering heat treatment on different isotropic specimens made of pure PTFE powder and compacted down to different values of the void ratio.

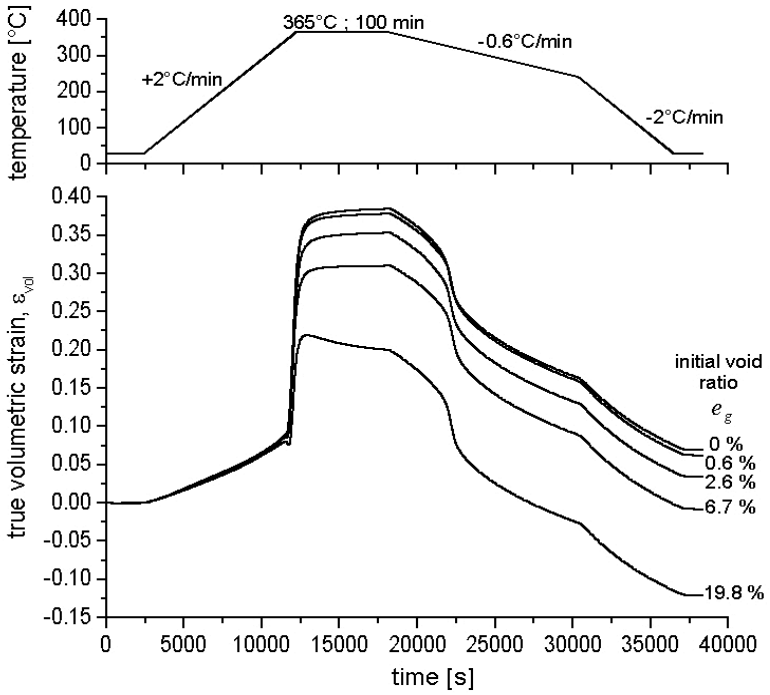

Figure 8 – True volumetric strain of isotropic specimens made of pure PTFE with different initial void ratios.

The reversible thermal strain before melting shows to be independent of the initial void ratio, which is in agreement with the behaviour of most porous materials.

The remnant volumetric strain at the end of the sintering process appears as equal to $\varepsilon_{vol} = +\,6.9\,\%$ for a nil initial void ratio specimen and $\varepsilon_{vol} = -\,12.1\%$ for a specimen with an initial void ratio equal to $e_g = 19.8\,\%$.

In general, the remnant volumetric strain after the sintering process is positive for specimens with low void ratio and negative for loose specimens. This phenomenon is related to the competition between a positive deformation mechanism due to the decrease of the crystalline weight fraction and a negative deformation mechanism due to the void closure during the heat treatment. Indeed, considering equations (8-9), the volumetric strain due to the variations of the crystalline weight fraction and void ratio during the sintering process can be derived from the following equation,

$$\varepsilon_{vol} = \ln \frac{v}{v_g} = \ln \frac{(\chi\ v_c + (1-\chi)\ v_a)\ (e+1)}{(\chi_g\ v_c + (1-\chi_g)\ v_a)\ (e_g+1)} \tag{11}$$

where index g refers to the green compacted powder. All plots given in Figure 8 correspond to a cooling rate of 0.6 °C/min and hence, according to equation (10), to a final crystalline weight fraction equal to $\chi = 0.42$ – whereas it is recalled that the initial value of the crystalline weight fraction is equal to $\chi_g = 0.89$. According to equation (11), the volumetric strain after sintering of fully dense material, i.e. with nil initial and final void ratios, $e_g = e = 0$, is equal to $\varepsilon_{vol} = 6.7$ % – to be favourably compared to the value of 6.9 % derived from the dilatometry test. The same equation applied to a specimen with an initial void ratio equal to $e_g = 19.8$ %, leads to a value of the volumetric strain equal to $\varepsilon_{vol} = -11.4\%$ – to be favourably compared to the value of – 12.1 % derived from the dilatometry test.

The variation with temperature of the specific volume of specimens with initial void ratios respectively equal to 0 and 19.8%, is compared in Figure 9.

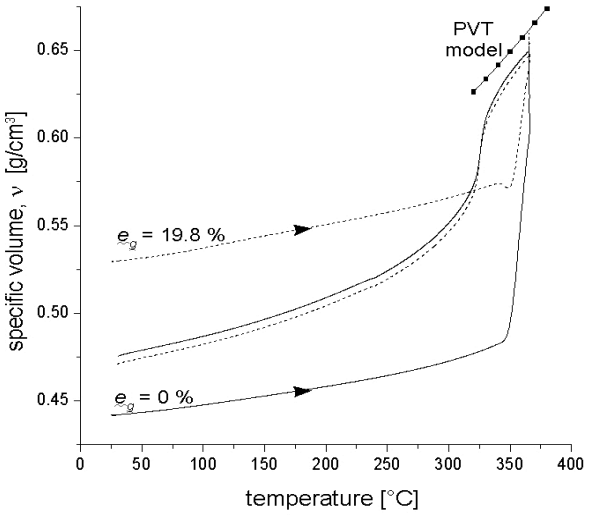

Figure 9 – Specific volume vs. temperature for two isotropic specimens of pure PTFE with different initial void ratios.

These plots show, firstly, that the void closure mechanism probably initiates after melting and secondly, that, whatever the initial void ratio of the green samples, void closure is almost complete after this typical sintering heat treatment. In other words, up to a certain limit, the final specific volume of homogeneous sintered samples is independent of their initial compaction. Although this is not the purpose of this paper, it was observed that the behaviour of the melt phase was in agreement with the Simha-Somcynsky equation of state 'PVT model' [26-27] fitted by parameters given in ref. [28].

3.4 Identification and modelling of void closure kinetics of pure PTFE

The strain associated to void closure, ε^{vcl}, can be derived from the results of dilatometry measurements made on different specimens subjected to the same heat treatment, so that

$$\varepsilon^{vcl}(t) = \varepsilon^{s}(t;\ e_g > 0) - \varepsilon^{s}(t;\ e_g = 0) \tag{12}$$

where ε^s *(t; e_g > 0)* and ε^s*(t; e_g = 0)* correspond to the time evolution of the total sintering strain of isotropic specimens with and without initial voids, respectively. Figure 10 illustrates this procedure when applied to a specimen with an initial void ratio, e_g, equal to 19.8%.

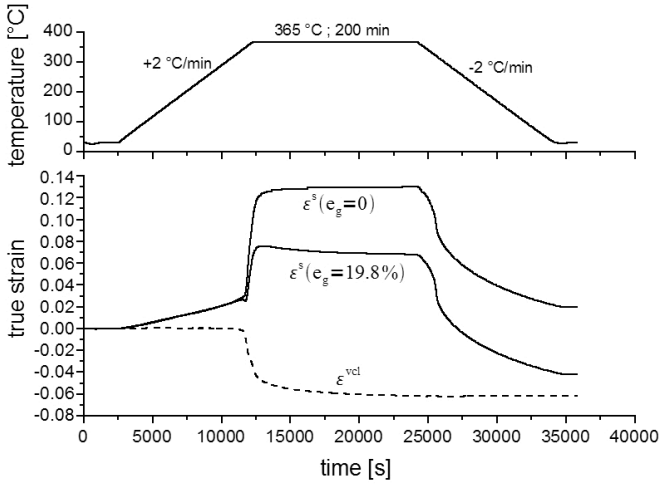

Figure 10 – Procedure to identify void closure strain in isotropic specimens.

It is recalled that dilatometry tests showed that void closure initiates during heating after melting of the crystalline phase has started. Melting temperature should be evaluated as the temperature, T_{onset}, at the beginning of the fusion peak as recorded during a standard DSC experiment. Herein, as a first approximation, it has been chosen that void closure starts when the fusion peak temperature, T_m = 344 °C, is reached, so that

$$\varepsilon_{vol}^{vcl} = \varepsilon_{vol}^{vcl}(t) = 0 \quad \text{when} \quad T(t) < T_y = T_m \tag{13}$$

Besides, since the sintering process stops when all voids are closed ($e = 0$), the final value of the strain associated to void closure can be derived from equation (11) as

$$\varepsilon_{vol\,\infty}^{vcl} = \varepsilon_{vol}^{vcl}(t_\infty) = ln\left(\frac{1}{1+e_g}\right) \quad \text{when} \quad T(t) \geq T_y = T_m \tag{14}$$

Different models have been proposed in the literature to model the void closure evolution (see for instance the review [29]). These models are based on various hypotheses and consider that the driving force for the coalescence of the pellets during sintering is a function of the surface tension and the viscous behaviour of the material. Considering the complexity of the mechanical state of compacted PTFE powder, it is proposed herein to model the void closure strain in isotropic specimens with the following purely phenomenological rate equation

$$\dot{\varepsilon}_{vol}^{vcl}(t) = a\,(\,\varepsilon_{vol\,\infty}^{vcl} - \varepsilon_{vol}^{vcl}(t)\,)\;H(T(t) - T_y) \tag{15}$$

where H is the Heaviside function and a a material dependent parameter. Considering the bounding values given by relationships (13-14), integration of evolution law (15) gives

$$\varepsilon_{vol}^{vcl}(t) = \varepsilon_{vol\,\infty}^{vcl}\;[\,1 - exp(-a\,t)\,] \quad \text{when} \quad T(t) \geq T_y = T_m \tag{16}$$

The material dependent parameter, a, was identified from dilatometry measurements performed on specimens with different initial void ratios subjected to the heat treatment depicted in Figure 10 so that value a = 0.001 of. The predictions of this model can be compared on Figure 11 with the experimental response of specimens with different initial void ratios subjected to different heat treatments. These results prove that, in this pure PTFE, the void closure mechanism is not very sensitive to the sintering temperature – within the range between 365 and 380 °C.

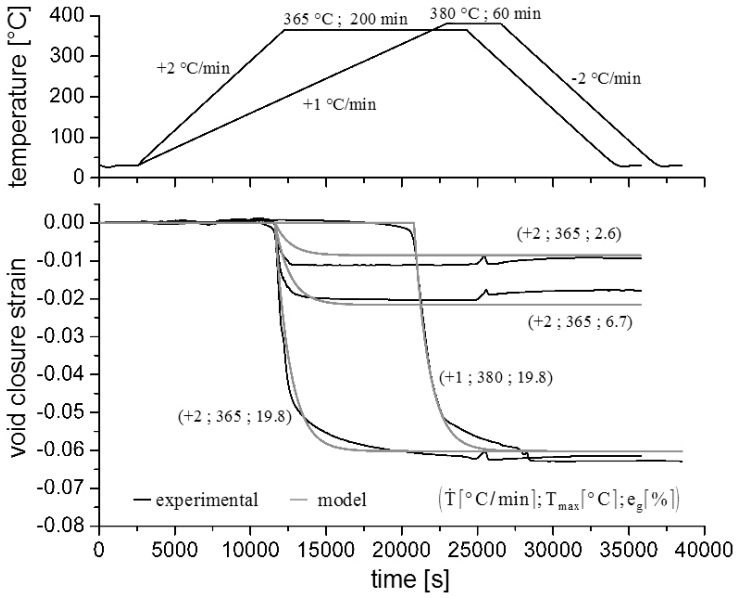

Figure 11 – Prediction of the strain associated to void closure (a = 0.001 and T_y = 344 °C).

4 Results obtained on anisotropic specimens

The results given in Figure 12 correspond to dilatometry tests which were performed while applying a typical sintering heat treatment on different anisotropic specimens (obtained by confined uniaxial compaction) made of pure PTFE powder and compacted down to different values of the void ratio.

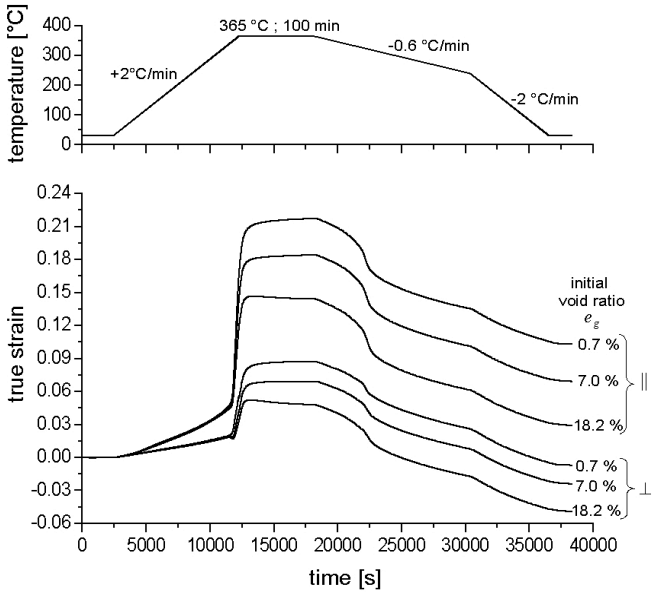

Figure 12 – True strain in the compaction direction, $\varepsilon_{\parallel}$, and in the transversal direction, $\varepsilon_{\perp}$, of anisotropic specimens of pure PTFE with different initial void ratios.

The variations of the strains during cooling of isotropic and anisotropic specimens compacted down to nil void ratio are compared in Figure 13. In this case, the reference length, L_i, is defined as the length of the specimen at the end of the dwell time at high temperature.

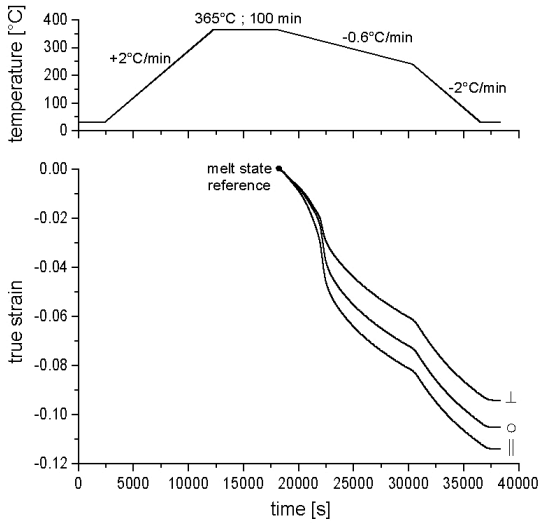

Figure 13 – Strains during cooling from melt reference state, of isotropic specimens, ε_o, and in the compaction direction, $\varepsilon_{\parallel}$, and in the transversal direction, $\varepsilon_{\perp}$, of anisotropic specimens of pure PTFE specimens with nil void ratio.

Besides, cyclic thermal tests – with a heating rate of + 2 °C/min, a cooling rate of – 2 °C/min, a 30 minute room temperature dwell time and a 60 minute dwell time at a maximum temperature that is increased at each cycle – were applied to pure PTFE specimens. The results of corresponding dilatometry measurements are given in Figure 14.

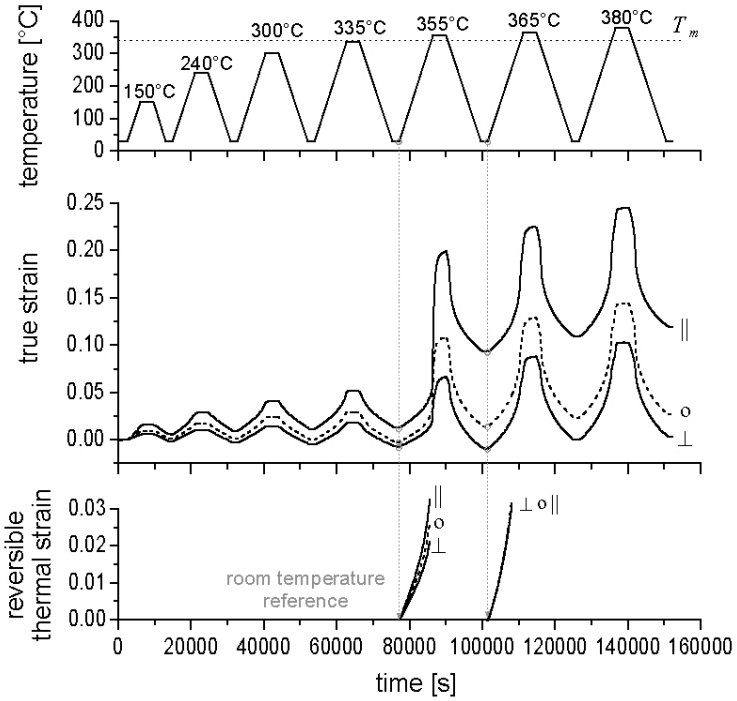

Figure 14 – Cyclic thermal tests up to a maximum temperature that is increased at each cycle – with constant heating rate of + 2 °C/min, cooling rate of – 2 °C/min, 30 minute room temperature dwell time and 60 minute dwell time at high temperature – applied to pure PTFE specimens with nil initial void ratio. True strain of isotropic specimens, ε_o, and true strain in the compaction direction, $\varepsilon_{\parallel}$, and in the transversal direction, $\varepsilon_{\perp}$, of anisotropic specimens.

The global behaviour of the specimens that were obtained by confined uniaxial compaction is strongly anisotropic, before and after melting. Competition between different strain mechanisms can be noticed.

The reversible thermal strain of the green pure material shows to be independent of the initial void ratio (see Figure 12) but anisotropic when the material is not hydrostatically compacted (see Figures 12 and 14). As a first approximation, whatever the compaction mode of the green material, the reversible thermal strain of sintered material, i.e. after melting and (partial) recrystallisation can be considered as isotropic (see Figure 14). Last, the thermal reversible strain also appears as being dependent on the crystalline weight fraction – be the specimens isotropic or anisotropic (see third plot on Figure 14).

Strains during cooling are due to two different mechanisms, viz. the crystallisation and the thermal contraction of the amorphous and crystalline phases. Since it has been shown that thermal contraction of sintered material is isotropic, crystallisation strain appears as being anisotropic in samples that were obtained by confined uniaxial compaction (see Figure 13). The most probable cause of this phenomenon is that the texture induced by the non-hydrostatic compaction is not fully erased by melting and that crystallisation depends on this remnant texture of the material after melting.

Reversible thermal expansion, void closure and crystallisation are not sufficient to explain the total deformation of anisotropic specimens during the sintering process (see Figure 14). Consequently, an additional deformation mechanism occurs. This mechanism is related to recovery and strongly depends on the non-hydrostatic strains that are induced by the compaction of the green

material. This phenomenon occurs at all temperatures but its variation with time is almost negligible below 75 °C, whereas it is particularly significant in the melt state.

5 Final remarks

The work presented herein is part of a study the aim of which is to better control PTFE powder processing and to predict the deformation of a component during the whole process, viz. powder compaction at room temperature and sintering heat treatment.

The results presented in this paper allowed to distinguish and identify different mechanisms that are responsible for the deformations of pure PTFE green parts during the sintering heat treatment. In isotropic green material – as obtained by isostatic pressing –, these strain mechanisms are respectively related to thermal expansion during heating, melting and void closure at high temperature, crystallisation and thermal contraction during cooling. In anisotropic green material, an additional recovery strain mechanism has been considered.

Finally, it is worth noticing that fillers induce additional anisotropies as illustrated by Figure 15. For instance, even the reversible thermal strain of filled PTFE is not isotropic after melting and (partial) recrystallisation.

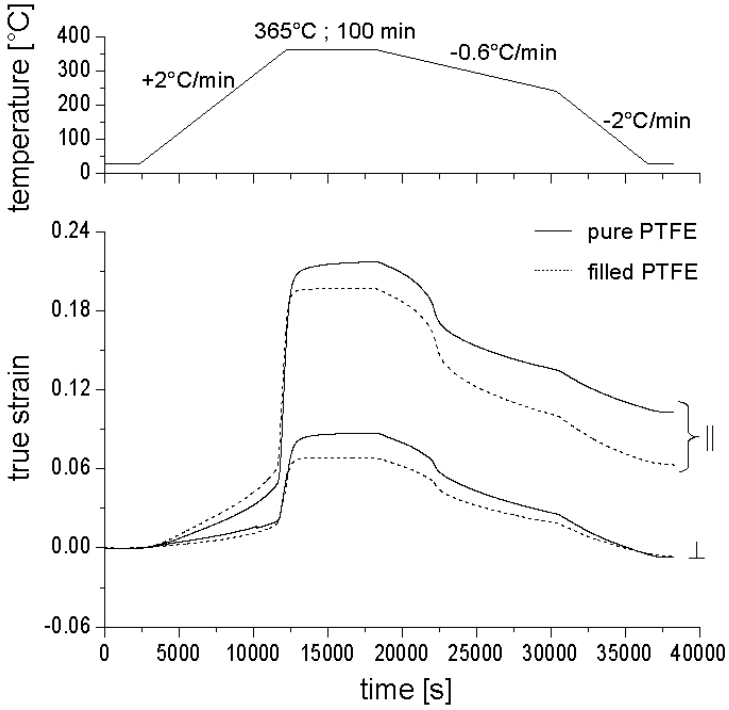

Figure 15 – True strain in the compaction direction, $\varepsilon_{\parallel}$, and in the transversal direction, $\varepsilon_{\perp}$, of anisotropic specimens of pure and filled PTFE with 0.7 % and 1.3 % void ratio, respectively.

6 Acknowledgements

The authors acknowledge the support of Tecnofluor Indústria e Comércio Ltda for providing the material. R.B. Canto acknowledges the support of the Conselho Nacional de Desenvolvimento Científico e Tecnológico – CNPq, of the Coordenação de Aperfeiçoamento de Pessoal de Nível

Superior - CAPES, and of the Fundação de Amparo à Pesquisa do Estado de São Paulo – FAPESP in Brazil, as well as the support of École Normale Supérieure de Cachan in France. The authors also acknowledge the LIM-ENSAM Paris and the IMA-Universidade Federal do Rio de Janeiro laboratories for the availability of DSC and TGA instruments.

7 References

[1] S. S. Hambir, J. P. Jog, V. M. Nadkarni, Strength development in powder processing of Poly(tetrafluoroethylene), Polymer Engineering and Science 34 (13) (1994) 1065–1069.
[2] L. W. Vick, R. G. Kander, Pressureless sintering of polycarbonate powder compacted at ambient temperature, Polymer Engineering and Science 38 (12) (1998) 1985–1996.
[3] J. P. Jog, K. R. Nath, V. M. Nadkarni, Solid-state processing of Poly(tetrafluoroethylene): simulation of sintering cycle, International Journal of Materials & Product Technology 9 (1-3) (1994) 155–169.
[4] R. J. Crawford, D. W. Paul, Y. Adeebnia, Microhardness and density distributions in polymeric powder compacts, European Polymer Journal 16 (1980) 401–405.
[5] R. J. Crawford, D. W. Paul, Radial and axial die pressures during solid phase compaction of polymeric powders, European Polymer Journal 17 (1980) 1023–1028.
[6] R. J. Crawford, Effect of compaction rate during the cold forming of polymeric powders, Polymer Engineering and Science 22 (5) (1982) 300–306.
[7] J. P. Jog, Solid state processing of polymers: A review, Advances in Polymer Technology 12 (3) (1993) 281–289.
[8] P. Gao, M. K. Cheung, T. Y. Leung, Effects of compaction pressure on cohesive strength and chain mobility of low-temperature compacted nascent UHMWPE, Polymer 37 (15) (1996) 3265–3272.
[9] N. Rosenzweig, M. Narkis, Observation and analysis technique for studying sintering of polymeric particles, Journal of Applied Polymer Science 26 (8) (1981) 2787–2789.
[10] C. T. Bellehumeur, M. K. Bisaria, J. Vlachopoulos, An experimental study and model assessment of polymer sintering, Polymer Engineering and Science 36 (17) (1996) 2198–207.
[11] C. T. Bellehumeur, M. Kontopoulou, J. Vlachopoulos, The role of viscoelasticity in polymer sintering, Rheologica Acta 37 (3) (1998) 270–278.
[12] S. Hambir, J. P. Jog, Sintering of ultra high molecular weight Polyethylene, Bulletin of Materials Science 23 (3) (2000) 221–226.
[13] A. Greco, A. Maffezzoli, Polymer melting and polymer powder sintering by thermal analysis, Journal of Thermal Analysis and Calorimetry 72 (3) (2003) 1167–1174.
[14] E. Scribben, D. Baird, P. Wapperom, The role of transient rheology in polymeric sintering, Rheologica Acta 45 (6) (2006) 825–839.
[15] N. A. Zubir, A. F. Ismail, Effect of sintering temperature on the morphology and mechanical properties of PTFE membranes as a base substrate for proton exchange membrane, Songklanakarin Journal of Science and Technology 24 823–831.
[16] L. Andena, M. Rink, F. Polastri, Simulation of PTFE sintering: Thermal stresses and deformation behavior, Polymer Engineering and Science 44 (7) (2004) 1368–1378.
[17] J.-F. Bonnet, Polymères fluorés, no. AM 3 390, Techniques de l'Ingénieur, 2004. *(in French)*
[18] D. Jahier, Le PTFE (Polytétrafluoroéthylène) : présentation et applications, Publications CETIM, 1992. *(in French)*
[19] P. J. Rae, D. M. Dattelbaum, The properties of Poly(tetrafluoroethylene) (PTFE) in compression, Polymer 45 (22) (2004) 7615–7625.

[20] H. Sun, R. S. Cooke, W. D. Bates, K. J. Wynne, Supercritical CO_2 processing and annealing of Polytetrafluoroethylene (PTFE) and modified PTFE for enhancement of crystallinity and creep resistance, Polymer 46 (20) (2005) 8872–8882.
[21] T. Tervoort, J. Visjager, P. Smith, Melt-processable Poly(tetrafluoroethylene) - compounding, fillers and dyes, Journal of Fluorine Chemistry 114 (2) (2002) 133–137.
[22] S. Kostromina, Y. Zubov, N. Shirina, Y. Tomashpol'skii, A structural investigation of the sintering of raw Polytetrafluoroethylene, Polymer Science U.S.S.R. 32 (2) (1990) 388–394.
[23] R. Androsch, B. Wunderlich, H. -J. Radusch, Analysis of reversible melting in Polytetrafluoroethylene, Journal of Thermal Analysis and Calorimetry 79 (3) (2005) 615–622.
[24] S. Ebnesajjad, Fluoroplastics Volume 1: Non-Melt Processible Fluoroplastics, 1st Edition, Vol. 1, William Andrew Publishing, Norwich, NY, 2000.
[25] D. M. Bigg, Study of effect of pressure, time, and temperature on high-pressure powder molding, Polymer Engineering and Science 17 (9) (1977) 691–699.
[26] R. Simha, T. Somcynsky, On the statistical thermodynamics of spherical and chain molecule fluids, Macromolecules 2 (4) (1969) 342–350.
[27] L. A. Utracki, R. Simha, Analytical representation of solutions to lattice-hole theory, Macromolecular Theory and Simulations 10 (1) (2001) 17–24.
[28] P. A. Rodgers, Pressure-volume-temperature relationships for polymeric liquids: A review of equations of state and their characteristic parameters for 56 polymers, Journal of Applied Polymer Science 48 (6) (1993) 1061–1080.
[29] E. A. Olevsky, Theory of sintering: from discrete to continuum, Materials Science and Engineering, R23, (1998) 41–100.